Annual Report 1999

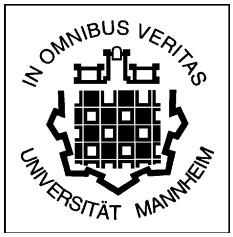

Chair of Optoelectronics
Faculty of Mathematics and Computer Science
University of Mannheim
B6,26
D - 68131 Mannheim
Telephone +49 (0)621 / 181 - 2704
Fax +49 (0)621 / 181 - 2695
EMail info@oe.ti.uni-mannheim.de
WWW http://www.ti.uni-mannheim.de/~oe

Micro-optics in Mannheim

Research continues in the field of optical interconnects and micro optics. The amount of work, however, seems to grow more rapid than the number of coworkers. Getting qualified students continues to be a problem in many German R&D institutions and also here at our chair. But at least for us, there is light at the end of the tunnel. Our first wave of students of the new course *Computer engineering* has now finished the seventh semester and we can expect a good number of new coworkers for a diploma thesis this year. The lecture *Introduction to Optics* is now held as a four our lecture and it was a gratifying experience to see, that the student's scientific fundaments meanwhile are solid enough to cover the full range of theoretical optics, ranging from Maxwell to Wigner.

The visit of Daniela and Mircea Dragoman ended in spring this year. The collaboration over a period of eighteen month was quite fruitful, resulting in five publications in the field of fractional Fourier transforms and related fields. In a collaboration with the institute for micro–technology Mainz (IMM), Jens Schulze has finished his PhD and presents the results of his work as contributions 12 and 13.

The project on angle multiplexing in fibers, although not yet being funded, is at the stage of being transferred to an industrial application. For an application to multi–layer optical connections within boards, a new type of multi–mode wave guide, the D-waveguides are investigated and vertical coupling has been demonstrated.

The post–diffusion process of ion–exchanged components plays a significant role in many of our projects, including continuous phase elements, long–focal–length micro lens arrays and optimized micro-optical systems. In contribution 7 Robert Klug has found, that the post–diffusion process can be modeled reliably with only one variable parameter, which is very helpful to perform component design numerically before a realization.

Funding in this year was dominated by industrial projects and we want to acknowledge collaboration with ABW, Perfect Vision, Rako-Electronic, Euromicron, Infineon, SL–Mikrotest and Thomson Multimedia. With the new year, a BMBF–funded project on optical disk readout will start and we are looking forward to an interesting and challenging project.

Karl-Heinz Brenner

Members of the chair of Optoelectronics

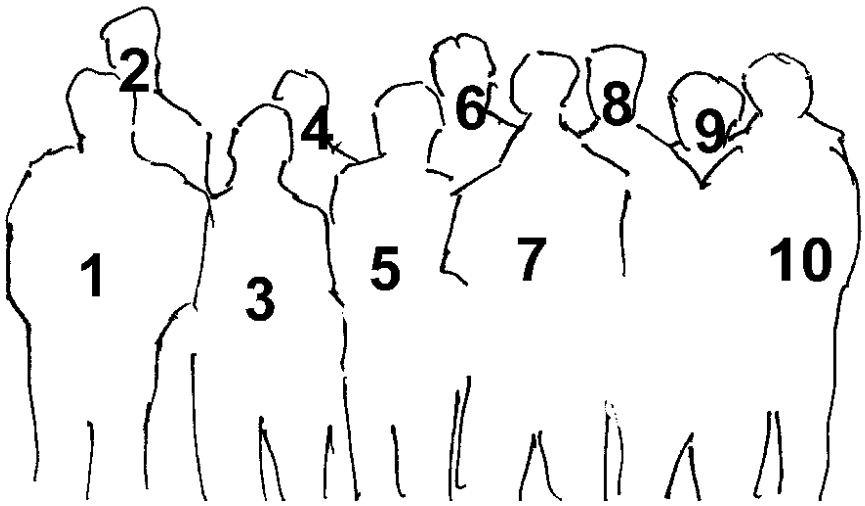

7	Dr. Bähr	Jochen	2694	jb@oe.ti.uni-mannheim.de
10	Prof. Dr. Brenner	Karl-Heinz	2700	brenner@uni-mannheim.de
1	Dengler	Christian		cdengler@rumms.uni-mannheim.de
	Dr. Dragoman	Daniela		dd@oe.ti.uni-mannheim.de
	Dr. Dragoman	Mircea		md@oe.ti.uni-mannheim.de
3	Fauland	Michael		fauland@rummelplatz.uni-mannheim.de
	Flammuth	Sven		flammuth@rumms.uni-mannheim.de
2	Fröning	Holger		maddock@rumms.uni-mannheim.de
9	Klug	Robert	2698	rklug@oe.ti.uni-mannheim.de
8	Dr. Krackhardt	Ulrich	2692	krackhdt@rumms.uni-mannheim.de
4	Kraft	Michael	2702	kraft@oe.ti.uni-mannheim.de
	Oberhöffken	Arndt		wwwadmin@oe.ti.uni-mannheim.de
6	Schmelcher	Thilo	2693	t.schmelcher@oe.ti.uni-mannheim.de
	Schulze	Jens		schulze.js@t-online.de
5	Volk	Sabine	2704	office@oe.ti.uni-mannheim.de

Contents

1 Fabrication of integrated D–Waveguide Y–branches by field assisted ion–exchange

T.Schmelcher, J.Bähr, K.-H. Brenner

In the past an emphasis has been on optical Wide Area Network communication. Due to the increasing demand for information bandwidth there is a growing interest for short range communication on the board and chip level. As an analogon to the printed circuit board we propose an „optical motherboard “. Basic elements for a typical interconnection scheme are point to point connections and branches. The information transport can be provided by vertically coupling. The multimode waveguides are fabricated with a field assisted silver–sodium ion exchange process in planar glass substrates. Due to the isotropic process the geometry of these waveguides is semi–cylindrical. In analogy to D–fibers [1] we use the expression D–Waveguides (D–WG). Furthermore such an interconnection system could act as an optical backplane with the possibility to couple vertically between two waveguide structures [2] with tolerant and efficient coupling interfaces.
Using different mask designs for the fabrication, point to point interconnections and y-branches can be realized. Steplike index variations within a glass substrate can be achieved by a field assisted ion exchange process [3][4]. For this process a planar glass substrate is coated with a titanium layer. This layer is structured photolithographically with a mask with line–shaped apertures. The glass substrate is placed into a melt of $AgNO_3$ and an additional electrical field is applied between the melt (anode) and the bottom of the glass substrate (cathode). At a temperature of about 300^oC, a current of silver ions drifts into the glass substrate. Simultaneously the sodium ions, initially present in the glass, move to the bottom electrode. Using line–shaped apertures with a small line width, the distribution of the electrical drift field and subsequently the distribution of the ions adopts a semi cylindrical shape. Figure 2 shows a cut through a D–WG element perpendicular to the cylinder axis. It verifies the cylindrical shape in good approximation.

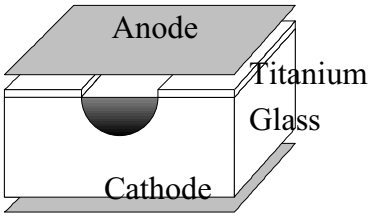

Fig. 1 Ion-Exchange Setup

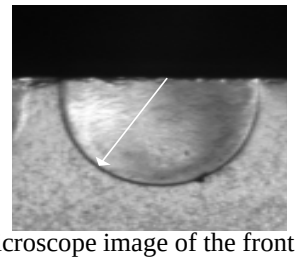

Fig. 2 Microscope image of the front face of a D-waveguide

For coupling into the D–waveguide we focussed a laser at the input plane. The output plane was monitored by a microscope setup with a CCD camera and a power meter.
In our first approach to realize a Y-branch we used a simple y-shaped mask. Figure 4 shows a magnified view of the branch point, looking from the bottom of the substrate. The yet unremoved mask appears as a black line. The opening angle of the Y-mask was 6 degrees. The diameter of the waveguide after exchange was 95 microns. The exchange was performed at a temperature of 300^oC and the applied electrical field was $125V/mm$. With this experiment we could obtain a symmetric splitting ratio of $50\% \pm 5\%$. The current investigation focus on attenuation and the minimum radius of curvature.

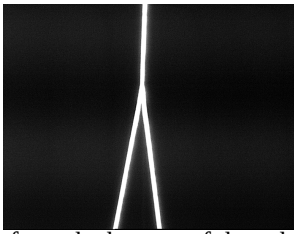

Fig. 3 View from the bottom of the substrat trough the Ti-mask

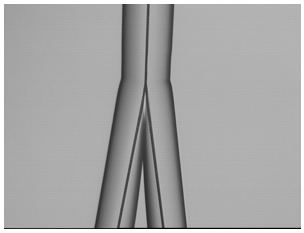

Fig. 4 View from the bottom of the glass substrat

References

[1] F. Mackenzie, R. Payne. D-fibre optical backplane interconnect. In *Proc. of SPIE*, **2153**, 218–226 (1994).
[2] J. Bähr, T. Schmelcher, K.-H. Brenner. Coupling of Multimode D–Waveguides page 5 Annual Report 1999.
[3] H.-J. Lilienhof, E. Voges, D. Ritter, B. Pantschew. Field-induced index profiles of multimode ion-exchanged strip waveguides. *IEEE Jour. of Quantum Electronics* **18**, 1877–1883 (1982)
[4] J. Bähr, K.-H. Brenner. Realization and optimization of planar refracting microlenses by Ag–Na ion–exchange techniques. *Appl. Opt.* **35**, 5102–5107 (1996)

2 Coupling of Multimode D-Waveguides

J. Bähr, T. Schmelcher, K.-H. Brenner

We proposed an interconnection scheme using special multimode waveguides, fabricated with a field assisted ion exchange process in glass. With this technique in addition to point to point interconnections also Y–branches for beam splitting [5] can be realized. Due to the special geometry of these waveguides, a simple and efficient connector system for vertically coupling between two waveguide structures can be attained by simply placing substrates on top of each other. The ratio of coupling can be adjusted tolerantly in a wide range. Such an interconnection system could act as an optical backplane with tolerant and efficient coupling interfaces.
For the fabrication we apply the field assisted silver–sodium ion exchange process in planar glass substrates. Due to this process the geometry of the waveguides is semi–cylindrical. In analogy to D-fibers [1] we use therefore the expression „D–waveguides“(D–WG).
The propagation in a D–WG is mathematically equivalent to propagation in a circular symmetric multimode fiber, since the surface of the glass virtually completes the D–WG to a full cylindrical waveguide by total internal reflection. Disturbing the condition for total internal reflection, light couples out of the bottom waveguide. A second identical D–WG placed on top of the first one can thus receive signal power from the bottom D–WG. Since the transversal modes are distributed statistically in a multimode waveguide, the maximum amount of energy in the second D–WG is 50%.

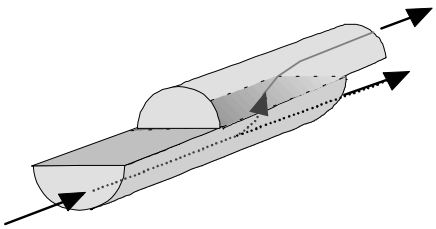

Fig. 1 Scheme of the coupling of two D-waveguides

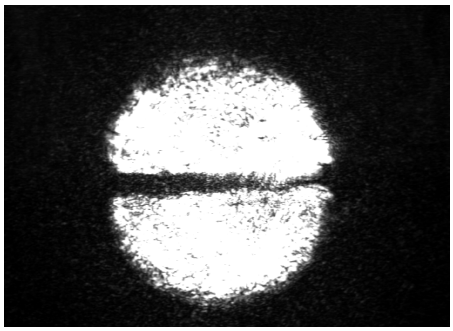

Fig. 2 Microscope image of the coupling experiment

For experimental verification we focussed a semiconductor laser ($\lambda = 635\ nm$) at the input plane of a D–WG structure. The output plane was monitored by a microscope setup with a CCD camera and a power meter. For vertical coupling we placed two substrates with identical D–WGs on top of each other. Both substrates were pressed together with a force of about 1 Newton. No index matching was applied. The diameter of the single D–WG was 95 μm, the pitch was 250 μm, the total length of both substrates was 20 mm. Light was coupled from the top D–WG to the bottom D–WG. The initial power in the top waveguide was measured and the power in the bottom waveguide was monitored. For testing the geometry for optimum coupling the following parameters have been varied: lateral shift and shear–angle between the substrates. The optimum coupling was found for the case of parallel orientation of the D–WGs, when the D–WGs were placed exactly on top of each other. Here a coupling of 40–50 % of the power was obtained. Figure 2 demonstrates a 50 % coupling from the top D–WG into the bottom one according to figure 1. Figure 2 shows a microscope image of the output planes of the stacked D–waveguides. Within a shear–angle of one degree a decrease of about 10 percent of the energy in the bottom substrate was obtained. With an shear larger than 3 degree from the parallel orientation the amount of coupling tended to zero. In the case of parallel orientation (0 degree), a lateral shift of 20 micron resulted in a 50 percent decrease of power in the bottom substrate. For measuring the excess loss, we compared the energy in the top substrate without coupling with that energy in the top and also in the bottom substrate at the optimum coupling geometry. We found an excess loss of less than 0.05 dB.
With this coupling technique a position- and angle tolerant connection for optical backplanes can be realized.

References

[1] F. Mackenzie, R. Payne. D-fibre optical backplane interconnect. In *Proc. of SPIE* **2153**, 218–226 (1994)
[5] T. Schmelcher, J. Bähr, K.-H. Brenner. Fabrication of integrated d–waveguide y–branches by field assisted ion–exchange, page 4, Annual Report 1999.

3 Improved mask design for the realization of micro lenses with long focal distances

J. Bähr. K.-H. Brenner, M. Fauland

We report the design and optimization of planar GRIN micro lenses by thermal ion exchange using a structured mask aperture. The micro lenses are fabricated with a diameter of 400 *µm* and numerical apertures in the range of 0.05 to 0.001 with diffraction limited performance. Special demand for these long focal length micro lenses has originated in the field of wave front sensors and in confocal microscopy.
In typical glass types, the thermal diffusion process through circular apertures results in index distributions, which are not suitable for high quality micro lenses. In preceding works we reported the use of concentric ring shaped mask structures to improve the phase profile [7]. These results have not been satisfactory, since the smallest feature size of 1.5 microns in the mask resulted in a minimum amount of ion concentration, which was not small enough to achieve a fine quantization. The phase shift resulting from a minimum feature size ring structure was only 60% of that using a full aperture. Due to this course sampling an additional post heating step had to be applied to smoothen the phase distribution, shown in figure 1.
To improve the quantization with respect to ion concentration we introduced an additional variation of the mask aperture within each single ring. The aperture density in angular direction acts as an additional degree of freedom in the mask design. Figure 2 shows a microscope image of the new mask structure. The structure was exposed into resist in a photolithographic process. To transfer the structure into the titanium mask layer a RIE process has been applied. With the new mask design we could improve the ratio of ϕ_{min}/ϕ_{max} to a value of 0.2. Due to that a more accurate sampling of the phase distribution was possible, and the additional post heating step could be omitted. Figure 3 demonstrates the quality of the phase distribution of a micro lens measured in a transmission interferometer. The deviation between the fit hyperbola and the real data is less than $\lambda/10$, resulting in diffraction limited performance over the entire aperture. Note also the congruence with the simulated data, shown in figure 3. The micro lens has a focal length of 5 *mm* and a numerical aperture of 0.05. Since the parameters are easy to control, the maximum deviation of focal length within an array of 400 elements was less than 1%. By variation of the mask design, the focal length can also be varied within a single substrate by a factor of 3.

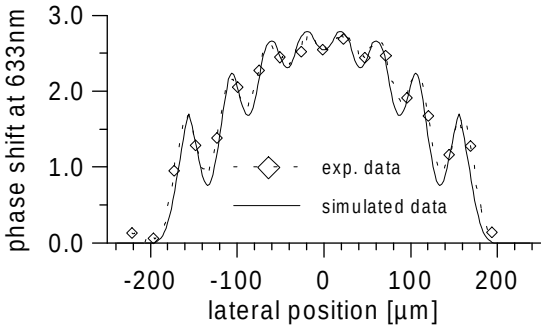

Fig. 1 Course sampling of the phase distribution using a ring shaped mask design; post heating is necessary

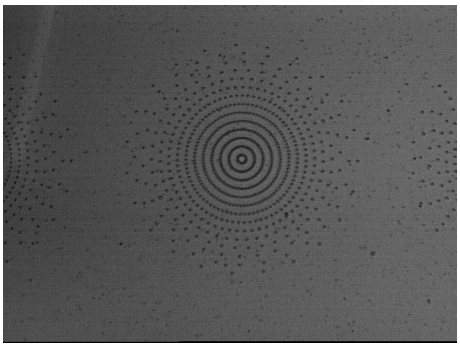

Fig. 2 microscope image of the titanium mask

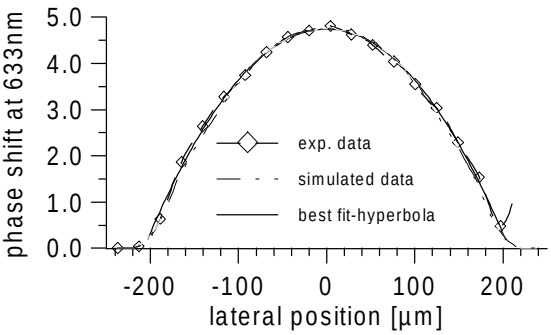

Fig. 3 Phase distribution using the new mask design

References

[6] K. Iga, M. Oikawa, S. Misawa, J. Branno and Y. Kokubun. Stacked planar optics: an application of the planar microlens. *Appl. Opt.* **21**, 3456–3460 (1982)
[7] J. Bähr, K. H. Brenner. Realization of planar microlenses with long focal distance by mask sysnthesis, page 7, Annual Report 1998.

4 Optical Set-up for relative Measurement of Tilt or axial Shift

U. W. Krackhardt

For some applications, e.g. motion control, it is important to keep track of the movement of parts of a system. Typically, only relative data is required. Here an optical set-up is proposed with the following properties [8]:
1) The same set-up can be used for both tilt and shift measurements, 2) the sensitivity is adjustable and 3) it offers a large measurement range (high space–bandwidth–product).

The idea is based on the fact that the principle propagation direction of a light ray within a multi-mode step-index fiber is conserved. Due to the cylindrical symmetry of a fiber, the azimthal angle is not conserved. As a result, one obtains a ring in the far field behind the fiber end. The radius of a ring corresponds to the coupling angle θ at the fiber input.
Fig. 2 shows a typical optical set-up which converts the coupling angle θ into a ring of radius R at a detector plane. Moreover, fixing θ and variing the distance d between the lens and the detector plane will also result in a variation of R. Consequently, a set-up as depicted in fig. 2 is suitable for acquiring both tilt *and* shift.
It is easy to see that the sensitivity of tilt measurements scales with d, whereas the sensitivity of shift measurements scale with θ. As a result, the role of measurement parameter and sensitivity parameter is interchanged when switching between tilt and shift acquisition. Since both θ and d can be continuously adjusted, sensitivity for each type of measurement can be set up.
As the size of the detector is limited, there is a trade–off between resolution and range. This trade–off can be overcome by applying multi–range techniques: The measurement parameter is replicated with different scaling, i.e. sensitivity. Subsequently, evaluation techniques like in multi–wavelength interferometry can be applied to obtain a highly resolved signal over a large range. Optically, the replication of the signal with different scaling is performed by a set–up as depicted in fig. 3: A computer generated hologram (CGH) magnifies of demagnifies the angle θ. This results in an up-scaled or down-scaled movement of a light spot over the detector plane while the measured parameter is variied. To this end the CGH is partitioned in different sectors. For illustration purpose, only two sectors are discussed here. The, say, upper sector perfoms a slow scaling of θ, the lower sector a fast scaling. The slow scaling is adjusted such that the detector area is sufficient for the entire measurement range. The fast scaling fits to the desired resolution. Also the fast scaling is designed such that the signal is always within the detector area. This is achieved by resetting the fast signal when the boarders of the detector plane are reached. There are various possibilities of implementing the scaling operations. One possible implementation is depicted in fig. 4 where the fast scaling ($f(\theta)$) is realized by a modulo operation. The transmission function $t(\rho,\varphi) = \exp(i\Phi)$ of the CGH can be defined in polar co–ordinates by $\Phi(\rho,\varphi) = s(\rho)\frac{r(1-2\sin(\varphi))}{R}$ or $\Phi(\rho,\varphi) = f(\rho)\frac{r\cos(\varphi)}{R}$ for the slow and fast scaling, respectively. R is the maximum radius defined by the extent of the detector and $s(\rho) = s_0 + s_1\rho$ or $f(\rho) = (f_0 + f_1\rho)\mathrm{mod}\rho_{\max}$ realize the appropriate scaling. As a result, the fast axis can by found on the detector plane along the $\varphi = 0$ direction and the slow axis along $\varphi = \frac{\pi}{2}$.

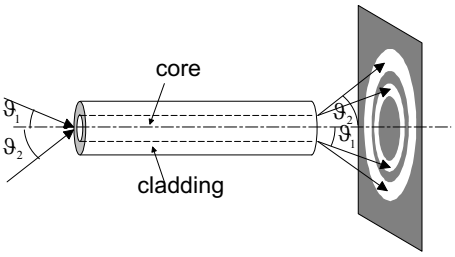

Fig. 1: conservation of principle propagation direction

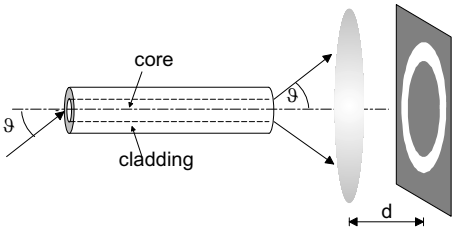

Fig. 2: optical set-up for alternatively sensing tilt or axial shift

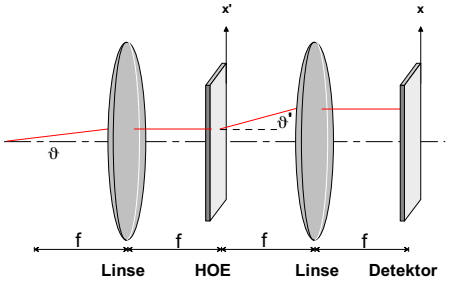

Fig. 3: optical set-up for replication and amplification of the coupling angle θ

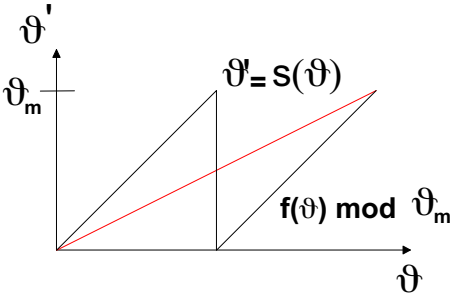

Fig. 4: Fast and slow scaling of the input angle θ.

References

[8] Krackhardt U., Brenner K.-H. Optischer Aufbau zur wahlweisen Distanz- und Winkelvermessung mit variabler Empfindlichkeit, 100. Jahrestagung der DGaO, Berlin 1999.

5 Micro–optical Calibration Object for one–shot absolute Calibration of Triangulation based optical 3D–Sensors with small Fields

U. W. Krackhardt

An optical triangulation sensor for acquisition of 3D–shape consists of $N > 2$ cameras inspecting the scene from different directions. Up to $N-1$ cameras may be replaced by projection units which may be considered 'inverse' cameras (structured light approach). In the following, cameras and projection units are both referred to as cameras. The range (depth) data is obtained by evaluating disparity or local shifts of a projected fringe pattern.In order to achieve precise co–ordinates, calibration objects are used for the characterization of a sensor (intrinsic parameters). If the co–ordinates are unique within the entire measuring volume (MV) the measurement technique is called absolute. For an absolute calibration the complete MV must be sampled by test objects with known relative positions. Due to the nature of triangulation not all test objects are visible for all cameras at the same time due to mutual blocking. Consequently, typical calibration procedures for absolute sensors are sequential.Here, an alternative approach is proposed which allows a parallel absolute calibration under certain circumstances [9]. The dilemma of mutual blocking of test objects can be loosened by the following considerations: 1) It is sufficient to perform a pairwise calibration for any two cameras of the sensor. 2) Mutual blocking is the more critical the more the viewing directions of the cameras differ (triangulation angle ϑ). From 1) it follows that a calibration object has to be designed only for two cameras. For consideration 2) there are practical applications like microscopic 3D-metrology which admit only small triangulation angles due to mechanical or optical constraints.

Considering microscopy it can be assumed that the inspection direction is perpendicular to the surface of the object under test. The triangulation angle is typically between 30 and 45 degrees.

A calibration object for parallel absolute calibration is sketched in fig. 1. It consists of N_z planes of glass which are stacked along the depth direction. Each plane holds a set of test objects. The location of the test objects is given by the non–blocking condition. This means that the test objects may not be aligned along the directions of view of any of the two cameras.

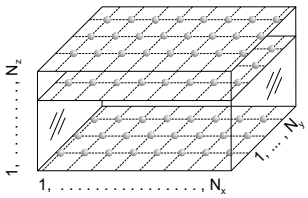

Fig. 1: Sketch of a calibration object for parallel absolute calibration

For a first step assume that all calibration objects are vertically aligned. In order for all objects of the top and the plane underneath to be visible for the vertical view the objects of the second plane must be laterally shifted. The amount of shift is limited by the non–blocking condition for the tilted inspection. Denoting the uniform lateral distance of objects by δx, the uniform separation of different planes by δz and the lateral shift of a plane by s, one obtains for a triangulation angle ϑ

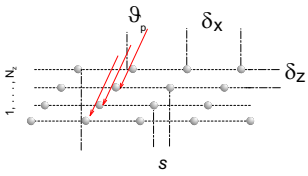

Fig. 2: Non-blocking constraint

$$s = \frac{\delta x - \delta z \tan(\vartheta)}{N_z - 1} = \frac{\frac{\Delta x}{N_x} - \delta z \tan(\vartheta)}{N_z - 1}.$$

Δx denotes the extent of the viewing field. N_x and N_z denote the number of test objects in a plane and the number of stacked planes, respectively. The calibration object is fabricated by lithographic techniques to obtain precise locations of the test objects within a plane. The planes are stacked with passive alignment achieving lateral accuracy of $\approx 5\mu m$.

For a practical example an active triangulation set–up is considered. The field extent is $\Delta x = 20mm$, the traingulation angle is $\vartheta = 45\,\mathrm{deg}$, the depth of the MV is $\Delta z = 2mm$ and the camera has 512 x 512 pixels. The period size Λ of the projected fringe pattern is sampled by 8 pixels, i.e. $\Lambda = \frac{\Delta x}{64} = 312\mu m$. The plane separation δz is set to the sensitivity $\varepsilon = 312\mu m$, i.e. to a distance which corresponds to a lateral shift of the pattern of one period Λ. One obtains $N_z = 7$ and for $N_x = 7$ there is a minimum shift of $s = 900\mu m$. That corresponds to an extent of 24 pixels per test object. This allows a coding of the test objects by bit-patterns. $B = \lceil \mathrm{ld}(N_x \cdot N_y \cdot N_z) \rceil$ bits are sufficient to uniquely address the test objects. For $N_x = N_y = N_z = 7$ it follows $B = 6$. The labels of the test objects can be read out by 2D–image processing. As a result, a parallel and automated calibration procedure is feasable.

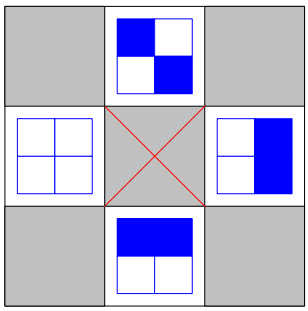

Fig. 3: Sketch of a coding scheme showing 4 coding and 5 measurement areas with the central area as the reference position

References

[9] U. Krackhardt, K.H. Brenner. Kalibriernormale für die bildgebende optische 3D–Messtechnik, 100. Jahrestagung der DGaO, Berlin 1999.

6 Forward Construction of HOEs by Continuous Aperture Division

U. W. Krackhardt, K.–H. Brenner

Typical design problems for holographic optical elements (HOE) are stated as follows: Given two distributions of light at an input and an output plane, find an appropriate HOE which transforms both distributions into each other. If the distributions are not completely specified (e.g. up to a phase), there is design freedom for optimization. Since propagation of light is involved, the design task is an inverse problem.
Basically, there are two optimization strategies: i) global and ii) sequential optimization.
i) All design parameters of the HOE are optimized simultaneously. This is appropriate if the design parameters are locally coupled by coherent light. For global optimization, iterative procedures like Iterative Fourier Transform Algorithms (IFTA) are applied. ii) If the design problem can be decomposed into sub–problems then sequential optimization on sub–spaces of the total parameter space is possible. In optical design, there are two strategies of decomposition: a) Multiplicative decomposition is typically performed on the component level by stacking optical elements and making use of the Kirchhoff approximation. Due to the propagation laws, convolution kernels have to be found to express the individual transmission functions. Consequently, this approach represents an inverse problem.
b) Additive decomposition is usually done on the field level, i.e. based on the interference of coherent light. A standard procedure is aperture division. The design parameters are coupled due to coherence and thus iterative optization techniques are required.
Here, we propose an alternative strategy [10]: Additive decomposition of the optical function on the component level. Additive techniques do not require deconvolution. Decoupling of design parameters is achieved by partially coherent illumination. This allows the use of generic primitives in the design procedure. As a consequence, sequential optimization enables a forward solution of inverse problems.
The HOE is divided into cells (**C**ontinuous **A**perture **D**ivision) by windowing. The window $w(x,y)$ is smooth and adjacent cells overlap. The window size is related to the correlation length of light, i.e. to the degree of coherence. The cells are placed on a continuous mesh.This approach can be considered an aperture division technique with continuous aperture boarders and locations. However, the entire aperture of the HOE is used for each elementary operation thus retaining image resolution of the complete HOE. The transmission function of the HOE can be written as

$$T(x,y) = \int\int \underbrace{t(x,y,x',y')}_{\text{partial solution}} \quad \underbrace{w(x,y,x',y')}_{\text{cell window}}\, dx'\, dy'.$$

In order to prove and illustrate the CAD–approach, an element for *parallel* optical generation of a spectrogram is considered: Given a structure $u(x)$ then $S(x,\nu) = |\int u(x')w(x-x')\exp(-2\pi i\nu x')\,dx'|^2$ is its spectrogram. At an output screen the spectral and the local information of $u(x)$ can be read off from the y– and x–axis, respectively. Standard methods are sequential: For each position x on the structure $u(x)$ the power spectrum is deflected onto a different y–location on a screen. The spectrogram is obtained by scanning the structure by moving an aperture window over the structure in x–direction while moving the screen in y–direction. Now, let the window function be gaussian, i.e. $w(x,x') = \exp[-\pi(\frac{x-x'}{\sigma})^2]$. Each cell realizes a different deflection, say, $\exp(2\pi i\alpha x'y)$. Then $T(x,y) = \int \exp[-\pi(\frac{x-x'}{\sigma})^2]\exp(2\pi i\alpha x'y)\,dx' = \frac{\sigma}{\sqrt{2\pi}}\exp(2\pi i\alpha xy)\exp[-\pi(\alpha\sigma y)^2]$ indicating that the sequential operation can be performed in parallel by one optical component.

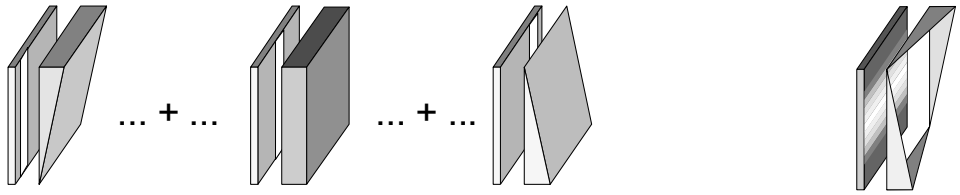

discrete superposition

result of continuous superposition

References

[10] U. Krackhardt, K.H. Brenner. Forward Construction of HOEs by Continuous Aperture Division. *Proc. Diffractive Optics*, 163–164, ISSN 1167-5357, Jena (1999)

7 Post-diffusion Model for the Index Profile of Ion-exchange Micro lenses

R. Klug, J. Bähr, K.-H. Brenner

In an earlier work [11] we have shown that index distribution of gradient index micro lenses can be optimized for a given imaging operation by a combination of field-assisted ion-exchange and an additional post heating step. By combining stacked layers of micro lenses, we have designed and optimized an array of multi-lens micro-systems [12]. From this work, we observed, that the quality of system modeling depends strongly on the exact knowledge of the index distribution of each single element. Most optical design tools use a polynomial for modeling the index distribution. As figure 1 shows, a polynomial fit of the order of 10 or even more is required for accurate description of the index shape. For the process of fields assisted ion-exchange, the index distribution is in good approximation rotationally symmetric. This symmetry is maintained during the post-diffusion process, but the maximum index and the shape of the distribution change significantly.

For a rapid optimization of stacked systems we need to use computer simulations. The parameters of the optimization process include the focal length, diameter, distance and the index distribution of each individual microlens. This index distribution is determined by a certain post heating duration. Consequently a model for the index distribution is needed, which is in sufficiently good agreement with the experimental data and which describes the index shape for a wide range of post diffusion times. Here we report on a unique model, which satisfies these requirements and in addition consists of only one free parameter.

The new model consists of a combination of a Lorentz function and a Fermi function:

$$\begin{aligned} M(r,\Delta n) &= \Delta n \cdot L(r) F(r) \\ &= \frac{\Delta n}{1+(br)^2} \frac{1}{1+exp(mr-\mu)} \end{aligned}$$

The Fermi function is useful for the description of step-like distributions. Together with the bell-shaped Lorentz-function, a good approximation to the experimental data was obtained. The parameters b, k, m, μ and also Δn change during the post diffusion process. By fitting many experimental index shapes to the model function M, we found a functional dependence between these parameters and the value of the maximum index difference Δn. With the knowledge of this functional dependence, the value of Δn is sufficient for the description of the complete shape of the index distribution.

Fig. 2 shows the radial index distribution for a very short post-diffusion time (a) and a very long short post-diffusion time (b). The agreement between experimental data (solid curve) and model (circles) is better than 1%. With this model, realistic micro optical system design can be performed with ray tracing software using only one parameter to describe the index shape. By a variation of the index shapes, system aberrations can be corrected.

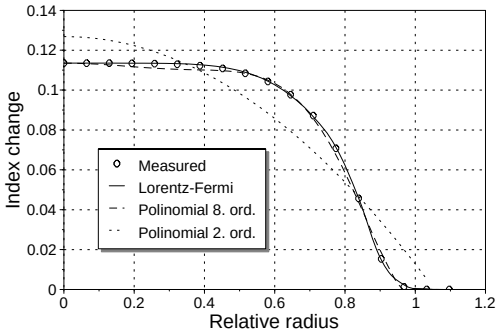

Figure 1. Models of the index distribution

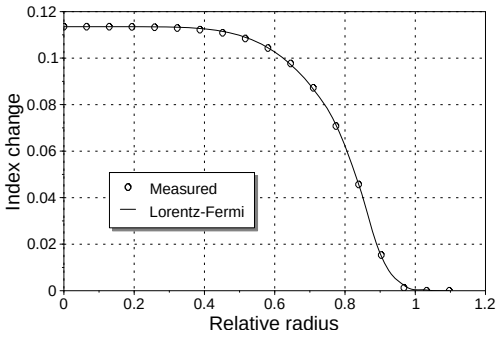

(a)

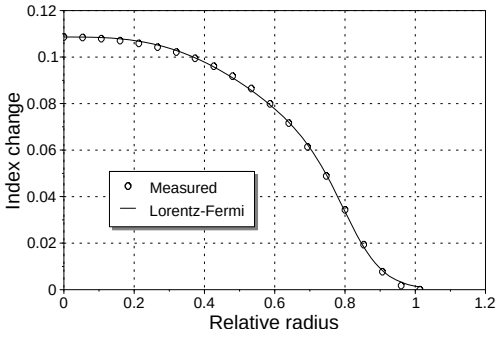

(b)

Figure 2. Lorentz-Fermi model describes accurate various index distributions

References

[11] J. Bähr and K.-H. Brenner. Realization and optimization of planar refracting microlenses by Ag–Na ion–exchange techniques. *Appl. Opt.* **35**, 5102–5107 (1996)

[12] R. Klug and K.-H. Brenner. Implementation of multilens micro–op systems with large numerical aperture by stacking of microlenses. *Appl. Opt.* **38**, 7002–7008 (1999)

8 Design of the MUX Unit for ADM–based Interconnects

R. Klug, U. W. Krackhardt

The MUX and DeMUX units are the key components of systems for multiplexed signal transmission. Under the constraints of the transmission medium, e.g. an optical fiber, the number of channels has to be optimized against cross–talk. In case of angle division multiplexing (ADM) [13], different locations of light sources and detectors have to be mapped to different propagation angles through a multimode step–index fiber.

The MUX and DeMUX units for ADM are passive optical components, thus no external electronic control is necessary. This facilitates micro-optical integration. In order to analize the feasibility of integration, alignment tolerances are studied. This article focusses on the design of the MUX unit. The scheme of the multiplexing device is shown on fig. 1. A system of micro lens and macro lens forms an imaging set-up for each channel with magnification β. A channel is input via a light source, here a monomode fiber (MOF). The angular volume (NA) of the multimode step–index fiber (MUF) is partitioned in disjoint angular intervals of size $\delta\theta_m$ centered at θ_m. Each channel is uniquely assigned to an interval.

The magnification β is determined by the NAs of the fibers: The NA of a micro lens must be greater or equal to the NA of the MOF and the NA of the macro lens must match the NA of the MUF. So, for a given pitch p of the input array, the focal length f_1 of a micro lens is given by $f_1 \leq p/NA(MOF)$. For a given number of channels N the focal length f_2 of the macro lens is given by $f_2 = \frac{(N-1)p}{2 \cdot NA(MUF)}$. Consequently, $\beta \geq \frac{N-1}{2} \frac{NA(MOF)}{NA(MUF)}$. Efficiency and tolerance requirements introduce an upper bound on β. Efficiency is mainly determined by insertion loss. A Gaussian beam with diameter D_M under oblique (θ) incidence at the interface of the MUF is considered. The core diameter of the MOF (MUF) is denoted by d_m (d_M). The coupling efficiency may be approximated by $\eta \approx 1 - \exp\left(-\frac{d_M^2}{D_M^2}\right) \frac{1+\exp(\sin^2\theta \cdot d_M^2/D_M^2)}{2}$ which limits D_M for a given $\eta_{\min}$. Since $D_M = \beta d_m$, the magnification is limited. Fig. 2 shows the insertion loss due to size mismatch for the worst case of oblique incidence at $\sin\theta = NA(MUF) = 0.48$. As a result, $\Delta\eta(D_M/d_M \approx 1.4) = -1dB$.

Within the scope of this article, a simplified tolerance analysis is carried out: The lenses are regarded as perfectly aligned. Alignment errors can thus only stem from the MOF and the MUF. Axial and lateral misalignment is investigated, only. Furthermore, the errors are assumed to be decoupled, i.e. not acting simultaneously. Lateral [axial] misalignment of the MOF scales with β [β^2] at the interface of the MUF. Thus, tolerance considerations of the MOF and MUF show the same results – proper scaling provided.

Lateral displacement of the MUF leads to a loss of coupling efficiency η. Fig. 3 shows the decay of η as a function of lateral displacement δx of a Gaussian beam at the fiber interface with $D_M/d_M = 1.5$. As a result, $\Delta\eta(\delta x/D_M \approx 0.6) = -1dB$.

Axial displacement has a negative impact on ADM transmission in two senses: a) The beam diameter scales with the distance δz from the waist. An axial shift of δz thus corresponds to a size mismatch. The impact of the change of beam diameter due to axial misalignment can be neglected. b) The curvature of the wave front scales with the distance δz from the waist. This leads to a larger angular extent per channel, thus increasing the cross–talk. In typical ADM applications the angular extent of a channel is $\approx 30\,mrad$. The divergence of a standard laser source is $\approx 3\,mrad$. So, an upper bound on the admissible curvature corresponding to a divergence of $3\,mrad$ is sensible. Fig. 4 depicts the admissible axial misalignment for a divergence of $3\,mrad$ at $\lambda = 850\,nm$.

A more elaborated tolerance analysis has been carried out by the authors. There, all degrees of freedom of the optical components were taken into account simultaneously. As a result of this analysis, an ADM interconnect over $L = 10m$ with $N = 10$ channels and 1.5 dB insertion loss and -10 dB cross-talk is feasible at $\pm 5\,\mu m$ fabrication tolerance of the mechanical support.

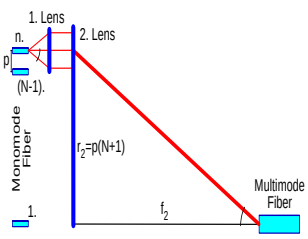

Fig. 1: Schematic set-up of the MUX device

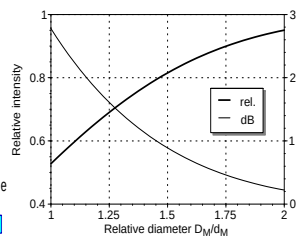

Fig. 2: Insertion loss due to size mismatch

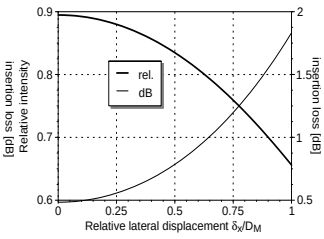

Fig. 3: Insertion loss due to lateral misalignment

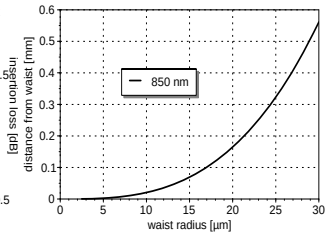

Fig. 4: Beam divergence due to axial misalignment

References

[13] U.W. Krackhardt, R. Klug and K.-H. Brenner. Broadband parallel-fiber optical link for short-distance interconnection with multimode fibers. *Appl. Opt.* **39**, 690–697 (2000)

9 Design of the DeMUX Unit for ADM–based Interconnects

R. Klug, U. W. Krackhardt, H. Fröning

As pointed out in an other contribution of this report [14], the MUX and DeMUX units are the key components of an ADM–based interconnect. The design constraints of the DeMUX unit are determined both by the alignment tolerances of the unit and by the transmission properties of the multimode step–index fiber. Since the tolerance analysis given for the MUX unit can be easily adapted to the DeMUX design, the transmission properties of the fiber are considered in this text. At the end of the multimode step–index fiber the light of the, say, m–th channel is coupled out at an angle θ_m with a finite angular width of $\delta\theta_m$. The DeMUX unit has to map different directions θ_m to different detectors.

One possible realization of the DeMUX unit is sketched in fig. 1 [13]. Light originating from the fiber end is collimated by the first lens. Thus, different directions are converted to different rings in the Fourier–plane of the first lens. In that plane, an optical element deflects the light of different rings into different directions. The second lens maps these directions to different locations in the detector plane. The angular width $\delta\theta_m$ is given by the quality and the length L of the fiber, as was first shown in [15]. Fig. 2 shows the measured output angle θ_m vs. input angle for a fiber with $d = 200\mu m$ core diameter, $N.A. = 0.49$ and $L = 1m$. A circle indicates the central angle of a ring. It can be seen that angle conservation is well fulfilled. The dashed curves depict the locations of the 1/e decay in the rings. From fig. 2 one can design a DeMUX with a given maximum cross–talk. If, for example, a cross–talk of -10 dB between adjacent channels is admissible, the annular rings must be separated by at least the 1/e–width. These locations can be read off from fig. 2. Because of design flexibility, a computer generated diffractive element (CGH) was used to realize the space–variant deflecting element. The CGH was partitioned in annular zones. In a first step the CGH was realized as an amplitude ronchi–ruled grating. The gratings in each zone differed in terms of period and tilt angle (fig. 3.a). Since the CGH was a binary amplitude hologram, there were unwanted diffraction orders. The CGH was designed such that only the, say, $+1^{st}$ diffraction orders coincide with the locations of the detectors. This has been achieved by arranging the $+1^{st}$ diffraction orders along a line well separated from the on-axis beam.

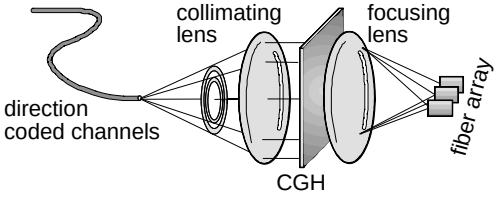

Fig. 1: Schematic set-up of the DeMUX device

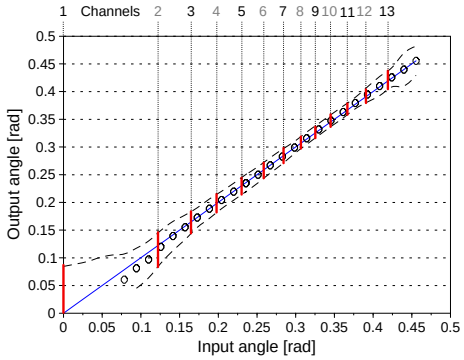

Fig. 2: Chart for the design of the channel positions

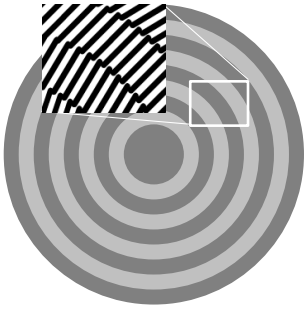

Fig. 3: a) Scheme of the ring grating

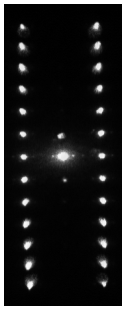

b) Far field of the CGH

Fig. 3.b shows a diffraction pattern of the CGH designed for 13 channels, when all channels were active. The cross-talk was measured with a 13 channel CGH designed according to fig. 2. The relative intensity coupled into an inactive channel from an adjacent active channel was taken as cross-talk. For an ADM transmission over 8m and 13 channels it turned out that only 4 channels show a cross-talk worse than -10 dB. This is due to the fact that the angular extent of the off-axis channels were assumed equal for ease of design. This was not exactly true as can be seen from figure 2. Higher cross-talk levels can be achieved by increasing the angular separation between the channels.

References

[13] U.W. Krackhardt, R. Klug and K.-H. Brenner. Broadband parallel-fiber optical link for short-distance interconnection with multimode fibers. *Appl. Opt.* **39**, 690–697 (2000)

[14] R.Klug and U.W. Krackhardt. Design of the MUX Unit for ADM–based Interconnects. page 11, Annual Report 1999.

[15] G. Glode. Optical power flow in multimode fibers. *Bell Syst. Techn. J.* **51**, 1767–1783 (1972)

10 Characterization of Fiber Parameters for Angle Division Multiplexing

R. Klug, U. W. Krackhardt and S. Flammuth

The figures of merit of a multiplexed transmission device are the number of channels and the cross–talk between the channels. Using angle divsion multiplexing (ADM) [13], the fiber quality and its resistance to environmental stress imposes a trade–off between the two figures. Poor fiber quality results in large angular spread of a channel, thus reducing the number of channels or increasing cross–talk.
As has been shown first by Glode [15] the fiber quality can be phenomenologically described by an analysis of optical power flow. As a result, energy propagating along a principal direction (mode) through a multimode step–index fiber diffuses into adjacent directions. The diffusion constant D is called 'coupling constant' in this context.

From a known D a tailored DeMUX unit can be designed as described on page 12 in this report [16]. As D is usually not provided by vendors, it has to be determined experimentally. Here, a procedure for measuring D of a particular fiber is described.
In the far field of the fiber end the intensity is distributed over a ring. The radius of a ring corresponds to the coupling angle θ_m, the thickness corresponds to the angular spread $\delta\theta_m$ resulting the finite angular spectrum of the light source, diffraction at the fiber interfaces and mode coupling. The latter effect scales with the propagation distance, thus limiting the interconnection length of ADM. Consequently, measuring $\delta\theta_m$ for various lengths L of a fiber allows the estimation of D. From [15] a simplified solution for the power distribution $p(\theta,z)$ of a beam propagating along the principle direction θ can be obtained for $D \cdot z \ll 1\,rad^2/m$:

$$p(\theta,z) = \exp\left(-\frac{(\theta-\theta_m)^2}{4D\cdot z}\right)\cdot\sqrt{\frac{4D\cdot z}{2\theta\cdot\theta_m}}$$

The angular distribution of the optical power has a Gaussian shape, centered at the principle propagation angle θ_m with a standard deviation $\sigma = \sqrt{4D\cdot z}$. As a result, the ring thickness scales with the square root of the length of the fiber. Thus, the coupling constant D can be obtained by a least–squares fit of the $\delta\theta_m$ for various fiber lengths. $\delta\theta_m$ was obtained by using a set–up as depicted in fig. 1:
A collimated laser beam was coupled into the multimode step–index fiber at an angle θ_m. At the fiber end the far field was observed by a camera. The thickness ($\propto\sigma$) of a ring was obtained by image processing. Fig. 2. shows the result for a standard multimode step–index fiber with numerical aperture $NA = 0.48$ and core diameter $d = 200\mu m$. From the fit $D = 6.7\cdot10^{-5} rad^2/m$ has been obtained.

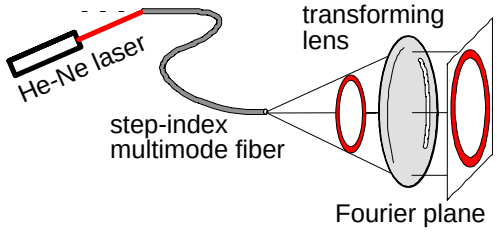

Fig. 1: Set-up for the measurement of fiber quality (D)

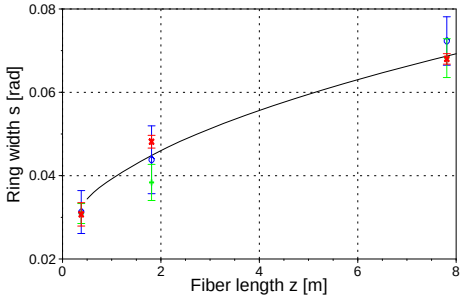

Fig. 2: Ring thickness vs. fiber length

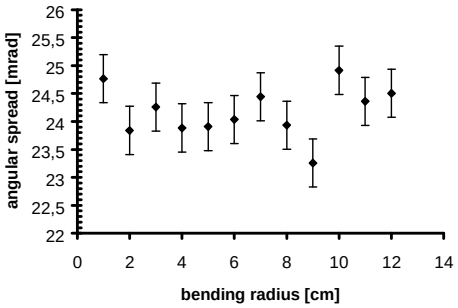

Fig. 3: Ring thickness vs. bending radius

With this set–up the sensitivity of ADM to macro bending has also been investigated. The thickness of a ring was measured vs. bending radius. Fig. 3. shows that thickness variations were below the resolution of the measurement equipment of $\pm 4\,mrad$. The angular extent of a channel is typically $30\,mrad$. As a result, ADM can be considered insensitive to macro bending.

References

[13] U.W. Krackhardt, R. Klug and K.-H. Brennerr. Broadband parallel-fiber optical link for short-distance interconnection with multimode fibers. *Appl. Opt.* **39**, 690–697 (2000)
[15] G. Glode. Optical power flow in multimode fibers. *Bell Syst. Techn. J.* **51**, 1767–1783 (1972)
[16] R.Klug, U.W. Krackhardt and H. Fröning, Design of the DeMUX Unit for ADM–based Interconnects, 1999. page 12 Annual Report 1999.

11 Method for designing arbitrary two-dimensional continuous phase elements

K.-H. Brenner

Diffractive optical elements play an important role in many applications ranging from laser beam shaping to optical free-space communication at the board or chip level. In order to achieve high diffraction efficiency, phase-only elements are preferable to amplitude elements. Among the class of phase-only elements, different types of phase profiles can be distinguished: binary phase elements, multi-level phase elements and continuous phase elements (CPE). Generally, the diffraction efficiency grows with the number of phase levels, favoring continuous phase profiles. A further advantage of CPEs is that for these types of elements no blaze condition exists. Therefore CPEs can be more tolerant to changes in incident angle and changes in wavelength. In spite of these advantages of CPEs two problems must be mentioned. The first concerns the fabrication process, which is typically analog. Therefore any process nonlinearies must be characterized and pre-compensated in the fabrication. The second problem concerns the design process. During the optimization of a phase element with an iterative Fourier transform algorithm, phase anomalies appear, which cannot be removed by continuation. The real- and imaginary part of the phase element are usually functions of position which are continuous and bipolar. Therefore the zero-crossings of both, $Re(x,y)$ and $Im(x,y)$ are lines in the x,y-plane. At the intersection of these zero-crossings, both, $Re(x,y)$ and $Im(x,y)$ are zero, resulting in a point-location where the amplitude is zero and the phase is undefined. Consequently, previous design methods were restricted to one-dimensional or, equivalently, to $x-y$–separable design intensities.
We have proposed a method for designing arbitrary two-dimensional continuous phase elements [17]. The phase anomalies due to amplitude zeros can be avoided with this method completely. Therefore the method is also useful for designing holographic elements which are free from amplitude zeros. The method is based on an iterative Fourier transform algorithm. In the iteration process, the method operates on the unwrapped phase. Consequently a subsequent continuation step is not needed. In the iteration we add corrections in the wrapped phase to the last version of the unwrapped phase. With this technique, continuous phase elements with a height variation exceeding 2π could be generated also for non-separable design intensities. These elements can be designed for a reconstruction in the zero-diffraction order. Therefore no carrier frequency is necessary. Furthermore, during all iteration steps > 1 the phase is always guaranteed to be continuous, by satisfying a phase gradient requirement compatible with the fabrication process.

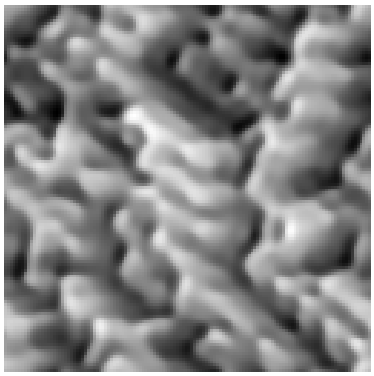

Fig. 1 continuous phase distribution

Fig. 2 reconstructed intensity

In order to demonstrate the potential of this new design method we used the letter F as a two-dimensional non-separable test distribution. The phase element was designed on a 128^2–grid with a definition window being 48x48 pixels in size. Fig. 1 shows the unwrapped phase as gray level distribution The maximum phase change here covers a range of 4.05π . In fig. 2 the reconstructed amplitude distribution is shown. It is normalized to the maximum amplitude.

After 2100 iterations the standard deviation was 7.3 % and the diffraction efficiency 77.5 %. The calculation time on a Pentium II, 350 was 15 min. With this method one of the mayor drawbacks of CPE's is removed. Since the method is based on an Iterative Fourier Transform Algorithm, also limitations of the fabrication process can be incorporated into the design. By enforcing, that the phase distribution is continuous, the amplitude of the computer generated element is guaranteed to be free of zeros which may also be of possible use for other applications.

References

[17] K.-H. Brenner. Method for designing arbitrary two-dimensional continuous phase elements. *Opt. Lett.*, **25** 31 – 33 (2000)

12 Parallel optical interconnects using self-adjusting microlenses on injection moulded ferrules made by LIGA technique

J. Schulze, M. Klaus[1]*, H. Müller*[1]

The miniaturisation of optical interconnections is an important aspect for the assembly of electro-optical devices. Two different parallel optical concepts for a multifiber access to such devices have been developed and realised using self-adjusting concepts with LIGA fabricated microstructures [18]. Using the butt coupling approach we fabricated an interface for hybrid integrated optical silicon based components. The passively mounted injection moulded interface achieves butt coupling between silica waveguides and fibers of the MT connector. Insertion loss values of less than 2.5dB were measured for singlemode transmission at 1300 nm wavelength [19]. Optical interconnection with a standardized multifiber connector and simplification in the packaging process are two main benefits of the described optical interface.
Parallel optical interconnets have also been realised with microlens arrays following the concept of expanded beam coupling. Two different types of connectors were therefore developed and realisied [20]. Type A connector uses an array of four biconvex contactless embosed microlenses ($d = 500\ \mu m$, PMMA, see report on page 16). In contrast, type B connector incorporates two conventional ball lenses ($d = 1\ mm$,glass: BK7) . For two optical channels we measured insertion loss values of $< 4,7$ dB (Type A) resp. $< 2,7$ dB (Type B) for multimode transmission at 1300 *nm*. Besides an application under harsh environmental conditions theses connector types could also act as building blocks for a variety of micro-optical devices.

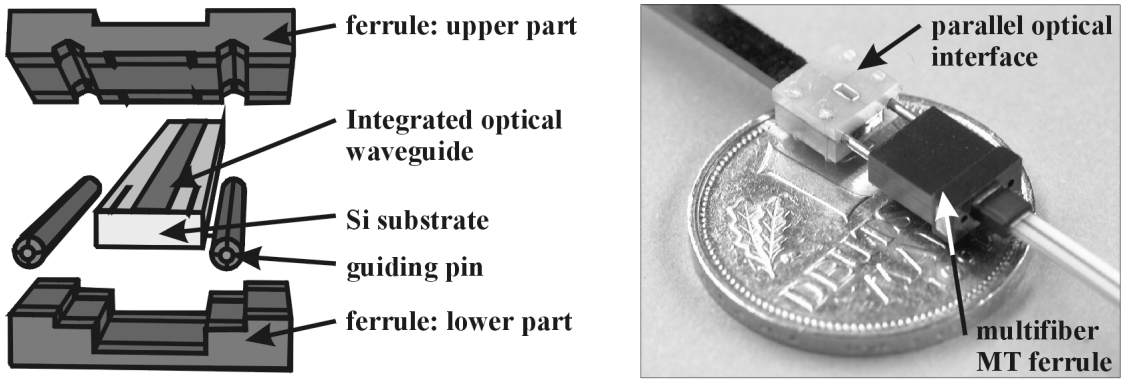

Fig. 1 (a) Mounting concept and (b) photograph of the interface connectorized with a multifiber ferrule

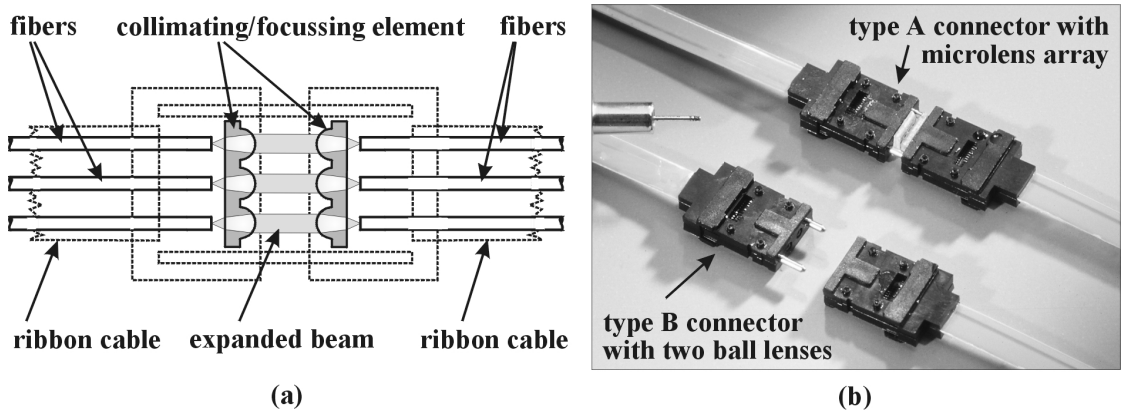

Fig. 2 (a) Schematic set-up and (b) photograph of the two prototypes of expanded beam connectors

References

[18] W. Ehrfeld, H. Lehr. Deep X-ray lithography for the production of treedimensional microstructures from metals, polymers and ceramics. *Radiat. Phys. and Chem.* **45**, 349-365 (1995)
[19] J. Schulze, W. Ehrfeld, J. Hoßfeld, H. Müller, A. Ambrosy, A. Picard. Parallel-optische Gehäuseschnittstelle für Optohybride. *ITG/VDE-Workshop: Phototonische Integration und Aufbautechnik, Nr. 19* (1999)
[20] J. Schulze, W. Ehrfeld, J. Hoßfeld, M. Klaus, M. Kufner, S. Kufner, H. Müller, A. Picard. Parallel optical interconnection using self-adjusting microlenses on injection moulded ferrules made by LIGA technique, *Proc. SPIE* **37**, No. 74 (1999) [A

[1]The authors are with Institut für Mikrotechnik Mainz GmbH (IMM), Carl-Zeiss-Straße 18-20, D-55129 Mainz (Phone: ++49-6131-990-0, Fax: ++49-6131-990-205, WWW: http://www.imm-mainz.de), where the technical project has been carried out.

13 Microlens arrays made of polymer material or glass through means of microtechnlogy

J. Schulze, M. Klaus[1]*, H. Müller*[1]

We report on two different fabrication techniques for refractive lenslets which have been investigated and characterised. The manufacturing method for microlenses made of a photosensitive glass material is known for photoform^{TM} glass (e.g. SMILE^{TM}) [1]. For a different glass (foturan^{TM} by Schott) we developed similar to this method a process to manufacture microlenses. Arrays of microlenses as shown in fig. 1 with lens diameter from 50 μm up to 1000 μm and a numerical aperture up to 0.13 have been fabricated using $5''$ wafers [2]. Investigations with a transmission interferometer show that according to the Rayleigh criterion the lenses provide diffraction limited performance within approx. 84 % of the aperture. High temperature stability up to 400C, cost effective production, and the possibility to apply additional photolithographic microstructures for alignment are the main advantages of microlenses made of foturan^{TM} glass. Contactless embossing of microlenses (CEM) is a modified moulding technique for fabrication of refractive microlenses. Applying precise LIGA microfabricated shims to the process a compact self-assembly of microlens arrays can easily be realised [3]. Arrays of microlenses as shown in fig. 2 with lens diameters from 30 m up to 1000 μm, both plan- and biconvex, with numerical aperture values up to 0.34 have been fabricated in transparent thermoplastics (e.g. PMMA). According to the Rayleigh criterion the microlenses provide diffraction limited performance within approximately 61% of the diameter. Self-assembly of these kind of microlenses in combination with injection moulded microstructures made by LIGA technique was successfully demonstrated by a prototype of an expanded beam connector (see report on page 15). Cost effective fabrication and the possibility to integrate optical and optomechanical functions for self-assembly makes these kind of microlenses interesting for many application fields, e.g. for use in fiber optical components.

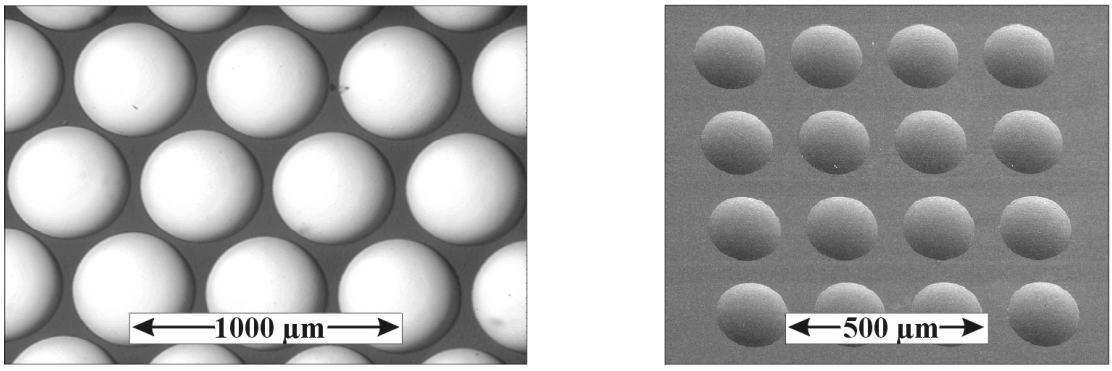

Fig. 1 (a) Microlenses made of foturan^{TM} $d = 460$ μm and (b) SEM image of lenses $d = 250$ μm

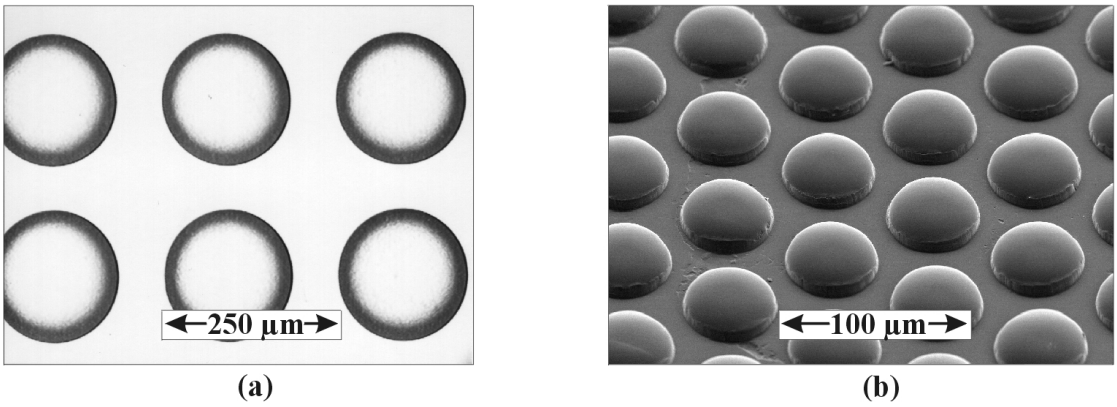

Fig. 2 (b) Contactless embossed lenses made of PMMA $d = 190$ μm and (b) SEM image of lenses $d = 50$ μm

References

[21] N. F. Borrelli. *Microoptics technology*. Marcel Dekker Inc., New York, 1999.

[22] A. Ambrosy et al. Grundlagen für eine optische Hybridtechnik, Optohybrid Abschlußbericht. Technical report, BMBF, 1999. ed. R. Schließer.

[23] J. Schulze, W. Ehrfeld, H. Müller, A. Picard. Compact self–aligning assemblies with refractive microlens arrays made by contactless embossing. In *Proc. SPIE* **3289**, 22–32 (1998)

[1]The authors are with Institut für Mikrotechnik Mainz GmbH (IMM), Carl-Zeiss-Straße 18-20, D-55129 Mainz (Phone: ++49-6131-990-0, Fax: ++49-6131-990-205, WWW: http://www.imm-mainz.de), where the technical project has been carried out.

14 Variant fractional Fourier transformer for optical pulses

D. Dragoman, M. Dragoman, K.-H. Brenner

In a previous work we have shown that a H-rod graded-index (GRIN) micro lens can perform the fractional Fourier transform (FRFT) of an incident beam with a continuously varying degree of fractionality along the meridional plane. To achieve this, the H-rod is illuminated off-axis and the output plane is its planar surface, i.e. an $x = const$ plane, in contrast to a full GRIN rod lens, where the output plane is a $z = const$ plane. The optical production of a FRFT with a continuously varying degree of fractionality is of practical importance especially for optical tomography applications, used for reconstructing the phase-space distribution (Wigner distribution) of the incident light field from the square modulus of the FRFTs with different degrees of fractionality. Other application where a FRFT with a variable degree of fractionality α is needed is the problem of estimation of the FRFT order.
Our purpose here was to find a method to produce a FRFT with a continuously varying degree of fractionality for optical pulses, instead of optical beams. In particular, we are looking for a method to produce the FRFT in the time domain instead of in the space domain. In order to achieve this goal, the analogy between the paraxial Fresnel diffraction and narrow band dispersion cannot be used in its present form because it refers to bulk optical elements, such as free space propagation and optical lenses. Therefore a temporal analogue for optical waveguides had to be developed. The goal was to find a medium in which the propagation of an optical pulse along the z-direction is described by the same differential equation as that of an optical beam in a H-rod microlens with a parabolic index profile:

$$\left(\frac{d^2}{dx^2} - (\beta^2 - k_0^2 n^2(x))\right)\phi(x) = \left(\frac{d^2}{dx^2} - [\beta^2 - k_0^2 n_0^2(1 - A^2x^2)]\right)\phi(x) = 0$$

The temporal counterpart would be a medium with a refractive index which has a parabolic dependence on time, but is linear for the propagating pulse. The method proposed in [24] is to choose a dispersive and nonlinear medium where the optical fields inside satisfy:

$$\left(i\frac{\partial}{\partial z} - \frac{\beta_2}{2}\frac{\partial^2}{\partial t^2} + k_0\Delta n(t)\right)u(t,z) = 0$$

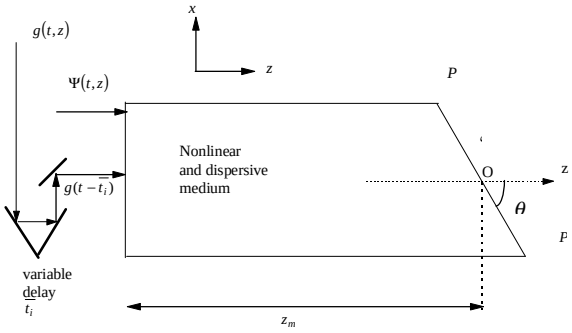

and to propagate, simultaneously with the optical pulse, a soliton pulse. In this equation, β_2 is the dispersion coefficient, t is the time coordinate in a system of reference which moves together with the pulse and Δn is the nonlinear part of the refractive index. The optical pulse must have a much lower intensity than the soliton such that it propagates linearly through the medium and the nonlinear refractive index is modulated by the soliton. This can be achieved if the peak power of the pulse is much larger than the product of the nonlinear coefficient of the medium and the propagation length. The off-axis excitation of a H-rod micro lens can be modeled in the temporal domain by a delay between the signal and the soliton and by making the observation at a $t = const$ moment.

This condition can be realized by obliquely cutting the end of the nonlinear medium and by making a snapshot recording of the pulse (see Fig.1). With this setup it is possible to perform a fractional Fourier transform with a continuously variant degree of fractionality in the time domain. The dispersive and nonlinear Kerr medium acts as a linear waveguide for the optical pulse and the refractive index is temporaly modified by a simultaneously launched bright soliton. Consequently, for optical pulses this medium is a perfect equivalent to a graded-index refractive medium for optical beams.

References

[24] K.-H. Brenner, D. Dragoman, M. Dragoman. Variant fractional fourier transformer for optical pulses. *Opt.Lett.* **24**, 933–935 (1999)

15 Experimental demonstration of a continuously variant fractional Fourier transformer

Daniela Dragoman, Mircea Dragoman and Karl-Heinz Brenner

In a recent contribution [25] we have proposed a first implementation of a fractional Fourier transform (FRFT) device with a continuously varying degree of fractionality. Such a device is of particular value in optical tomography. We have extended the 1D theory presented in [25] to a 2D theory and we have performed experiments which demonstrate that an off-axis illuminated hemispherical rod (H–rod) microlens acts as a FRFT transformer of continuous degree of fractionality [26]. The working principle is based on the fact that the degree of fractionality α of the fractional Fourier transform is determined (as in a GRIN full rod) by the distance z covered by the ray inside the H–rod (see Fig.1a and Fig.1b) with a refractive index which can be approximated by.

$$n(x,y) = n_0\left[1-\left(\frac{A^2}{2}\right)(x^2+y^2)\right] \quad x <= 0$$

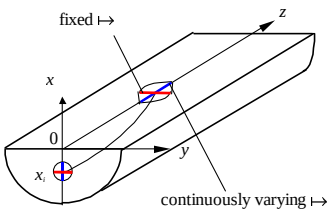

Fig. 1a Geometry of a HROD micro lens

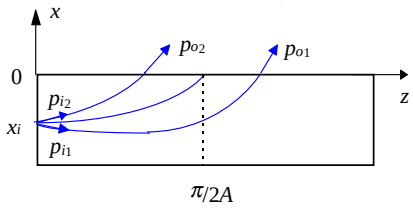

Fig. 1b Rays in the meridional plane incident under different angles

So, the expected results are:

1. a FRFT with a variable α in the meridional plane which at the distance $z = \alpha\pi/2A$ is given by:

$$\tan\left(\frac{\alpha\pi}{2}\right) = -n_0 A\frac{x_i}{p_i}$$

where x_i are the excitation positions and p_i the excitation angle. The constants n_0 and A have typical values of 1.544 and $6.510^{-4}\mu m^{-1}$ respectively and the H–rod used in the experiment had a radius of $450\mu m$.

2. a FRFT with constant α in the sagital plane.

In Fig.2a and 2b the calculated and measured light intensities are represented for an illumination with a mono–mode optical fiber which provides an incident Gaussian light beam with a width $w = 50\mu m$, $x_i^- = 400\mu m$ and $p_i^- = 0$. The α range is: $0.5 - 1$.

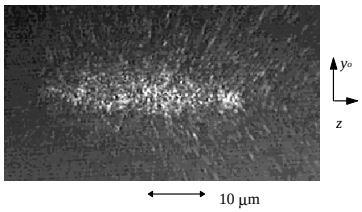

Fig. 2a Measured output light intensity for an incident Gaussian beam

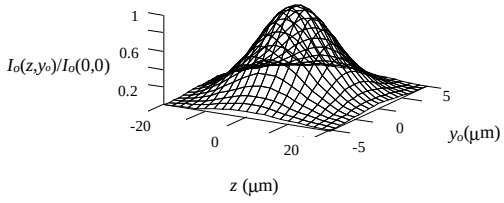

Fig. 2b Calculated output light intensity for an incident Gaussian beam

References

[25] D. Dragoman, K.-H. Brenner, M. Dragoman, J. Bähr, U.W. Krackhardt. Hemispherical-rod microlens as a variant fractional fourier transformer. *Opt. Lett.* **23**, 1499 – 1501 (1998)
[26] D. Dragoman, M. Dragoman, K.-H. Brenner. Experimental demonstration of a continuously variant fractional fourier transformer. *Appl. Opt.* **38**, 4985 – 4989 (1999)

A List of recent Publications

68. K.-H. Brenner, U. Krackhardt. Komponenten und Aufbautechniken für mikro-optische Systeme zur Informationsübertragung. *it+ti* **41**, Nr. 6, 39–48 (1999)

69. R. Klug, U. Krackhardt, K.-H. Brenner. Richtungsmultiplex für optische Verbindungen zwischen Platinen. Tagungsbeitrag ORT 98 Paderborn.

70. D. Dragoman, M. Dragoman, J. Bähr, and K.-H. Brenner. Phase space measurements of micro-optical objects. *Appl. Opt.* **38**, 5019–5023 (1999)

71. R. Klug, U. W. Krackhardt, K.-H. Brenner. Angular Multiplexing for optical Board to Board Interconnections. In Optics in Computing, OSA Technical Digest, 118–120, Snowmass 1999.

72. U. Krackhardt, K.-H. Brenner. The Berry-Phase applied to optical Metrology. In *Proc. of the Workshop on Physics in Computer Science*, ed. Werner Kluge, 177–185, Heidelberg (1999)

73. D. Dragoman, M. Dragoman and K.-H. Brenner. Experimental demonstration of a continuously variant fractional Fourier transformer. *Appl. Opt.* **38**, 4985–4989 (1999)

74. R. Klug, K.-H. Brenner. Implementation of multilens micro–optical systems with large numerical aperture by stacking of microlenses. *Appl. Opt.* **38** 7002–7008 (1999)

75. D. Dragoman, M. Dragoman and K.-H. Brenner. Variant fractional Fourier transformer for optical pulses. *Opt.Lett.* **24**, 933–935 (1999)

76. K.-H. Brenner, R. Klug and U.W. Krackhardt. Angle division multiplexing in multi-mode fibers for optical board-to-board interconnection. *SPIE*, eds P.Réfrégier, B. Javidi, Euro-American Workshop on Optoelectronic Information Processing, Critical Review, **CR74**, 61–69 (1999)

77. U.W. Krackhardt, R. Klug, K.-H. Brenner. Broadband parallel-fiber optical link for short-distance interconnection with multimode fibers. *Appl. Opt.* **39**, 690–697 (1999)

78. K.-H. Brenner, R. Klug and A. Knüttel. Microoptic Implementation of an Array of 1024 Confocal Sensors. In *OPTO '98 Proceedings*, AMA Fachverband für Sensorik, 155–160, Erfurt 1998.

79. K.-H. Brenner, U.W. Krackhardt, R. Klug. Directional Multiplexing for optical Board to Board Interconnections. In *Proc. of SPIE*, Optics in Computing '98, **3490**, 416–418, Bruegge 1998.

80. J. Bähr, K.-H. Brenner. Optical motherboard: a planar chip to chip interconnection scheme for dense optical wiring. In *Proc. of SPIE*, Optics in Computing '98, **3490**, 419–422, Bruegge 1998.

81. K.-H. Brenner. Analysis of phase anomalies and design of continuous phase elements. *Diffractive Optics '99*, EOS Topical Meeting Digest Series, 22, 22–23 ISSN 1167–5357, Jena 1999

82. U. Krackhardt and K.-H. Brenner. Forward construction of HOE's by continuous aperture division. *Diffractive Optics '99*, EOS Topical Meeting Digest Series 22, 163–164 ISSN 1167–5357, Jena 1999

83. K.-H. Brenner. Method for designing arbitrary two–dimensional continuous phase elements. *Opt. Lett.* **25**, 31–33 (2000)

84. U. W. Krackhardt, R. Klug, K.-H. Brenner. Faser–optische Kurzstreckenverbindungen zur breitbandigen und parallelen Signalübertragung. Tagungsbeitrag ORT 99 Jena, Band 4, 10–15 ISSN 1437–8507, 1999.

85. J. Bähr, K.-H. Brenner, J. Moisel, W. Singer, S. Sinzinger, T. Spick and M. Testorf. Modification of the image properties of ion–exchange microlenses by mask shaping. In *Technical Digest of the 10. Topical Meeting on Gradient–Index Optical Systems EOS*, 187, Santiago de Compostela, Spain 1992

86. K.-H. Brenner U. Krackhardt. Absolutes flächenhaftes Interferometer. patent pending, DE 198 33 291 A1, IPC G 01 B 9/02, 1998

Publisher: Lehrstuhl für Optoelektronik
Fakultät für Mathematik und Informatik
Universität Mannheim
B6, 26
D–68131 Mannheim
Germany

Tel: +49 (0)621 181–2704
Fax: +49 (0)621 181–2695
Mail: info@oe.ti.uni-mannheim.de
WWW: http://www.ti.uni-mannheim.de/~oe

Editor: Dipl.–Ing. Thilo Schmelcher

Tel: +49 (0)621 181–2693
Mail: t.schmelcher@oe.ti.uni-mannheim.de

Print: Universitätsdruckerei Mannheim